UC Berkeley
UC Berkeley Previously Published Works

**Title**
Piezoresponse amplitude and phase quantified for electromechanical characterization

**Permalink**
https://escholarship.org/uc/item/3fg0v3d1

**Journal**
Journal of Applied Physics, 128(17)

**ISSN**
0021-8979

**Authors**
Neumayer, Sabine M
Saremi, Sahar
Martin, Lane W
et al.

**Publication Date**
2020-11-07

**DOI**
10.1063/5.0011631

Peer reviewed

eScholarship.org Powered by the California Digital Library
University of California

Journal of Applied Physics

# Piezoresponse amplitude and phase quantified for electromechanical characterization

Cite as: J. Appl. Phys. **128**, 171105 (2020); https://doi.org/10.1063/5.0011631
Submitted: 24 April 2020 . Accepted: 10 October 2020 . Published Online: 05 November 2020

Sabine M. Neumayer, Sahar Saremi, Lane W. Martin, Liam Collins, Alexander Tselev, Stephen Jesse, Sergei V. Kalinin, and Nina Balke

View Online
Export Citation
CrossMark

Meet the Next Generation of Quantum Analyzers
And Join the Launch Event on November 17th

Zurich Instruments

© 2020 Author(s).

Journal of Applied Physics | TUTORIAL | scitation.org/journal/jap

# Piezoresponse amplitude and phase quantified for electromechanical characterization

Cite as: J. Appl. Phys. **128**, 171105 (2020); doi: 10.1063/5.0011631
Submitted: 24 April 2020 · Accepted: 10 October 2020 ·
Published Online: 5 November 2020

View Online
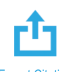
Export Citation

CrossMark

Sabine M. Neumayer,[1] Sahar Saremi,[2,3] Lane W. Martin,[2,3] Liam Collins,[1] Alexander Tselev,[4] Stephen Jesse,[1] Sergei V. Kalinin,[1] and Nina Balke[1,a)]

## AFFILIATIONS

[1]Center for Nanophase Materials Sciences, Oak Ridge National Laboratory, Oak Ridge, Tennessee 37831, USA
[2]Department of Materials Science and Engineering, University of California, Berkeley, Berkeley, California 94720, USA
[3]Materials Sciences Division, Lawrence Berkeley National Laboratory, Berkeley, California 94720, USA
[4]Department of Physics and CICECO-Aveiro Institute of Materials, University of Aveiro, 3810-193 Aveiro, Portugal

[a)]**Author to whom correspondence should be addressed:** balken@ornl.gov

## ABSTRACT

Piezoresponse force microscopy (PFM) is a powerful characterization technique to readily image and manipulate the ferroelectric domains. PFM gives an insight into the strength of local piezoelectric coupling and polarization direction through PFM amplitude and phase, respectively. Converting measured arbitrary units into units of effective piezoelectric constant remains a challenge, and insufficient methods are often used. While most quantification efforts have been spent on quantifying the PFM amplitude signal, little attention has been given to the PFM phase, which is often arbitrarily adjusted to fit expectations. This is problematic when investigating materials with unknown or negative sign of the probed effective electrostrictive coefficient or strong frequency dispersion of electromechanical responses, because assumptions about the PFM phase cannot be reliably made. The PFM phase can, however, provide important information on the polarization orientation and the sign of the effective electrostrictive coefficient probed by PFM. Most notably, the orientation of the PFM hysteresis loop is determined by the PFM phase. Moreover, when presenting PFM data as a combined signal, the resulting response can be artificially lowered or asymmetric if the phase data have not been correctly processed. Here, we explain the PFM amplitude quantification process and demonstrate a path to identify the phase offset required to extract correct meaning from the PFM phase data. We explore different sources of phase offsets including the experimental setup, instrumental contributions, and data analysis. We discuss the physical working principles of PFM and develop a strategy to extract physical meaning from the PFM amplitude and phase.

*Published under license by AIP Publishing.* https://doi.org/10.1063/5.0011631

## I. INTRODUCTION

Progress in many areas of science is indelibly linked to advances in techniques to investigate the functional behavior on the micro- and nanoscale that have become essential in materials science and device engineering. Among these characterization techniques in areas such as ferroelectricity, energy storage and conversion, and information technologies, some important advancements are related to the development of piezoresponse force microscopy (PFM) and PFM switching spectroscopy modes.[1–15] These techniques allow for the study of piezoelectric and ferroelectric activities on the micro- and nanometer scale via detection of mechanical response to electric fields applied to the sample via a cantilever-shaped conductive probe. PFM is widely available due to the commercialization of many atomic force microscopy manufacturers and has become a popular tool within the materials-science community. However, not only is the technique inherently prone to artifacts to be aware of, but correct processing and interpretation of PFM signals are not always straightforward. This leads to two important challenges the PFM is facing. The first one is reliable and consistent measurements of piezoresponse, which are often displayed in arbitrary units only making it hard to compare results of different research groups, obtained with different instruments as well as data across literature on the same material systems. The second is the quantification of functional material properties from PFM data, namely, the extraction of piezoelectric tensor components, which includes complications associated with inhomogeneous electric fields around the biased PFM tip and local


Published under license by AIP Publishing.

mechanical clamping. While the latter has been partially described in the literature,[16,17] the first challenge still needs to be addressed. This is important because the extraction of material properties relies on the correct handling and quantification of PFM data. Some of the critical considerations to achieve this goal are universal and do not depend on how PFM is performed, which include the correlation of the PFM signal and probed functional material property. Others apply only to specific implementations, such as the resonance-enhanced PFM, where the signal-to-noise ratio is improved by exciting the cantilever probe to vibrate in resonance at its first flexural eigenmode.[18] In this case, single frequency PFM can be subject to sample topography crosstalk resulting in artificial PFM contrast, which can be avoided by an application of multi-frequency PFM, including dual resonance frequency tracking[11] and band excitation.[18] Other challenges for resonance-enhanced PFM involve ruling out the effects of electrostatic forces or other non-electromechanical phenomena as predominant signal origins[19,20] and the convolution of cantilever beam shape and the measured PFM signal which can be mitigated by employing interferometric sensing approaches.[21,22]

In this tutorial, we focus on the PFM configuration that measures the periodic surface displacement along the normal to the sample surface as a result of oscillating volume changes induced by an AC voltage $V_{ac}$ applied to the probe tip in contact with the sample surface in respect to a bottom electrode. We chose the laboratory reference system so that the $z$ axis is directed outward, or "upward," from the sample. Electric fields or polarization directions pointing in the positive direction of $z$ are defined as positive. If they are pointing in the direction of negative $z$, or downward, they are defined as negative. The sample height change is tracked by a change in cantilever inclination near the probe tip, which is measured with the help of a reflected laser beam and a photo-detector, whose signal $D$ (termed deflection) is represented in volts. The resulting oscillating deflection $D_{ac}$, which can be termed "rate of deflection," is proportional to the changes in the slope of the cantilever[23,24] caused by the oscillating height changes of the sample normal to the sample surface $\Delta L_z = (L_z - L_0)$, where $L_z$ denotes the bias-induced and $L_0$ denotes the unbiased sample (or effective probing) thickness. It is standard in microscopes that a positive $D$ indicates a shift of the sample surface up in the positive $z$-direction (that is, $\Delta L_z > 0$ if $D > 0$) and vice versa. With a strain $S_z = \Delta L_z/L_0$ and an electric field approximation $E = -V/L_0$, where $V$ is the voltage applied to the probe (and, therefore, has the sign opposite to the direction of $E$ with respect to the $z$ axis), the PFM signal can be used to obtain information about the piezoelectric properties along the normal to the sample,

$$d_z = \left(\frac{\partial S_z}{\partial E_z}\right) = -\left(\frac{\partial \Delta L_z}{\partial V_z}\right) = -K \cdot \frac{D_{ac}}{V_{ac}}. \quad (1)$$

Here, $K$ is a proportionality factor that relates the measured deflection rate $D_{ac}$ in volts to the surface displacement $\Delta L_z$ in pm and has the unit pm/V. Note that if the voltage is applied to the bottom electrode, the "minus" sign in Eq. (1) should be replaced with "plus." Since the PFM probes the surface expansion and contraction in the laboratory reference system along the normal of the sample surface ($z$-direction), which does not necessarily align with the sample crystallographic axes, PFM is often described as probing an "effective piezoelectric constant" that we denote here with $d_z$. This property contains contributions of multiple components of the third rank piezoelectric tensor $d_{ijk}$ that depend on inhomogeneous electric field distribution around the biased PFM tip with in-plane and out-of-plane field components and on the crystallographic orientation of the sample with respect to the surface normal. The detailed discussion of PFM signals in the presence of vertical and in-plane field components for samples of different crystallographic orientations can be found elsewhere.[25–27] In the following, the focus is on reliable and correct extraction of $d_z$ (the effective piezoelectric constant); the extraction of the $d_{ijk}$ tensor components from measured values of $d_z$ is not discussed here.

There are challenges when it comes to reliably measure and extract the PFM amplitude $A$ and phase $\phi$ of the dynamic deflection rate $D_{ac}$. The PFM amplitude is proportional to the effective piezoelectric constant along the normal of the sample surface, while the phase has directional information on the polarization orientation. The PFM phase is the phase lag between the applied voltage on the probe and the measured strain response extracted with lock-in or related methods. Often, the PFM amplitude and phase are combined to yield a so-called mixed response $D_{ac}$ that is defined as $D_{ac} = A \cdot \sin(\phi)$ or $D_{ac} = A \cdot \cos(\phi)$. While there have been efforts to quantify the PFM response to extract $d_z$ from $D_{ac}$,[28–33] the fact that $d_z$ and $D_{ac}$ are opposite in sign if the PFM tip is biased as shown by Eq. (1) is typically not considered. The sample piezoresponse amplitude is often quantified simply by the cantilever static deflection sensitivity $S_c$ in pm/V, which is only a factor in $K$ in Eq. (1). At the same time, little attention has been paid to the correct PFM phase, although this parameter yields valuable information on fundamental physical properties such as the sign of the electrostrictive coefficients and frequency dispersion of electromechanical response. The PFM phase is either used as measured or sometimes adjusted to maximize the mixed-PFM response so that $\sin(\phi)$ or $\cos(\phi)$ equals $\pm 1$ and/or according to the expected loop orientation. Some notable exceptions are of Chen *et al.* who calibrated the phase response in electrochemical strain microscopy against PFM phases measured on ferroelectric samples with known polarization and electrostriction coefficients[34] and Bradler *et al.* who proposed a phase calibration and correction method based on numerical calculations.[35]

Many factors determine the measured PFM phase and often include unknown contributions, which can lead to oppositely oriented PFM phase loops in the literature on the same material system.[36–40] Even measurements using the same sample and microscope can result in oppositely oriented loops, as demonstrated in Fig. 1. Here, the switching spectroscopy was performed using resonance-enhanced PFM on a standard ferroelectric $PbZr_{0.2}Ti_{0.8}O_3$ (PZT) sample using soft (spring constant $k = 4.2$ N/m) and stiff ($k = 45.6$ N/m) cantilevers with free (out-of-contact) resonance frequencies of 72 kHz and 165 kHz, respectively, and contact resonance frequencies of about 330 kHz and 625 kHz, respectively. The PFM amplitude and phase were extracted using a simple harmonic oscillator (SHO) fit of the voltage-dependent contact resonance peak (as explained below). It can be seen that the PFM amplitudes measured in pm/V, after



Published under license by AIP Publishing.

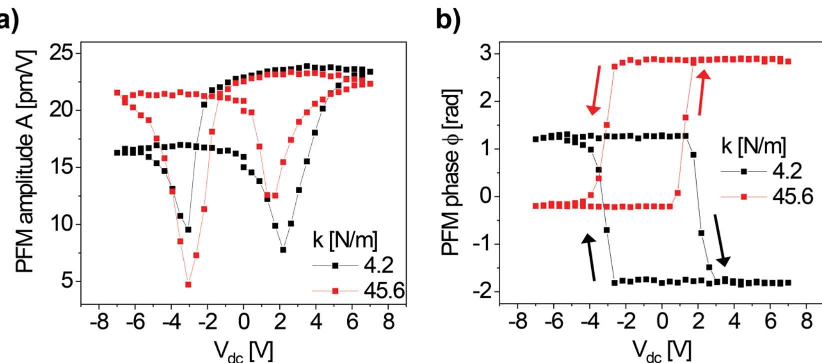


**FIG. 1.** PFM (a) amplitude and (b) phase loops measured on the same sample with a soft (4.2 N/m, black) and stiff (45.6 N/m, red) cantilever using resonance-enhanced PFM. The contact resonance frequency for these cantilevers was ∼325 kHz and ∼625 kHz, respectively. The amplitude was quantified using cantilever sensitivity. The phase loops show opposite orientations.

multiplication of the detector signal by cantilever sensitivity $S_c$, depend on the cantilever [Fig. 1(a)], which has also been reported in Ref. 41. The orientation of the as-measured phase loops is opposite to one another, which would result in oppositely oriented $D_{ac}$ loops [Fig. 1(b)]. In addition, the uncorrected phase levels for these two loops vary greatly. These observations are unexpected since the same material property is probed which should be independent of the used cantilever if the applied fields are comparable. If the phase is not correctly processed before calculations of the mixed response, $D_{ac}$ can appear lower (e.g., if cos ($\phi$) < 1 and > − 1) and information provided by the loop orientation is lost or misleading. Therefore, clear guidelines need to be established on how to correctly process the PFM phase if no assumption about the loop orientation can be made. This is especially important for materials that exhibit negative electrostriction coefficients as, for example, observed in PVDF[42] and $CuInP_2S_6$.[43,44] Similarly, for materials with mobile ions or low-frequency polarization dynamics, the significant dispersion of electromechanical responses can be expected in the range of frequencies amenable to PFM, necessitating quantitative absolute phase measurements.

In the following, we address a big challenge for PFM-reliable and reproducible measurements of the effective piezoelectric constant and hysteresis loops. As demonstrated in Fig. 1, this requires evaluation of common quantification steps, and we explore in detail more advanced approaches to correctly quantify the PFM amplitude and identify the PFM loop orientation as determined by the PFM phase. We discuss the presence of instrumental phase offsets and their frequency dependence as a main contributor to the measured PFM phase. We will also discuss some specific challenges that on-resonance PFM methods face, which includes considerations of cantilever dynamics, the signal-to-noise ratio, and fitting procedures before the PFM amplitude and phase are received. We will demonstrate how the phase offset can be determined based on the physical meaning of the PFM phase, which will be demonstrated on a $PbZr_{0.2}Ti_{0.8}O_3$ (PZT) thin film. The developed procedure will then be applied to $CuInP_2S_6$, a ferroelectric material with a negative electrostrictive tensor component along the direction of the probed strain,[43,44] which yields the loop orientation opposite to that of traditional ferroelectrics such as PZT.[42,43,45]

## II. RESULTS AND DISCUSSION

First, we discuss the ideal PFM hysteresis loop and how the effective piezoelectric response relates to the orientation of the polarization (with respect to the applied field direction) and the electrostrictive coefficient. In the laboratory reference system, the effective piezoelectric response can be described by the following equation:

$$d_z = 2Q_z P_z \varepsilon_z \varepsilon_0. \tag{2}$$

According to Eq. (2),[46,47] the effective piezoelectric constant $d_z$ is determined by the effective electrostrictive coefficient $Q_z$ and the polarization vector component along the laboratory coordinate $z$, $P_z$. Therefore, the measured effective piezoelectric response can be positive or negative depending on the sign of $Q_z$ and the orientation of $P$. Electrostriction, in general, is described by a fourth rank tensor $Q_{ijkl}$, which describes the relationship between strain and the square of the polarization, $S_{ij} = Q_{ijkl}P_kP_l$. This means that electrostriction itself does not depend on the sign of polarization.

Figures 2(a) and 2(b) show the ideal PFM amplitude and phase hysteresis loop depicted for a ferroelectric material like PZT. The DC voltage is applied to the PFM tip; therefore, a positive voltage will result in a negative field direction, which orients the polarization downward (the red arrow in Fig. 2); in turn, a negative voltage will switch the polarization upward (the blue arrow in Fig. 2). The PFM amplitude is always positive, has two positive branches that partially overlap, and contains no information about the polarization direction [Fig. 2(a)]. This is different for the PFM phase that probes the direction of the polarization with respect to the applied field direction [Fig. 2(b)]. When the polarization and the field vector point are in the same direction, an increase in field will result in an increase in polarization and material expansion if the electrostrictive coefficient is positive. In that case, the field and the strain increase at the same time and are in-phase with each other and the PFM phase is $\phi = 0$. Opposite to that, when the polarization and the field vector point are in opposite directions, an increase in field will result in a decrease in polarization and material contraction if the electrostrictive coefficient is positive. In that case, a field increase results in a strain decrease, and they are out-of-phase with each other and the PFM phase is $\phi = 3.14$ ($\pi$) rad.


Published under license by AIP Publishing.

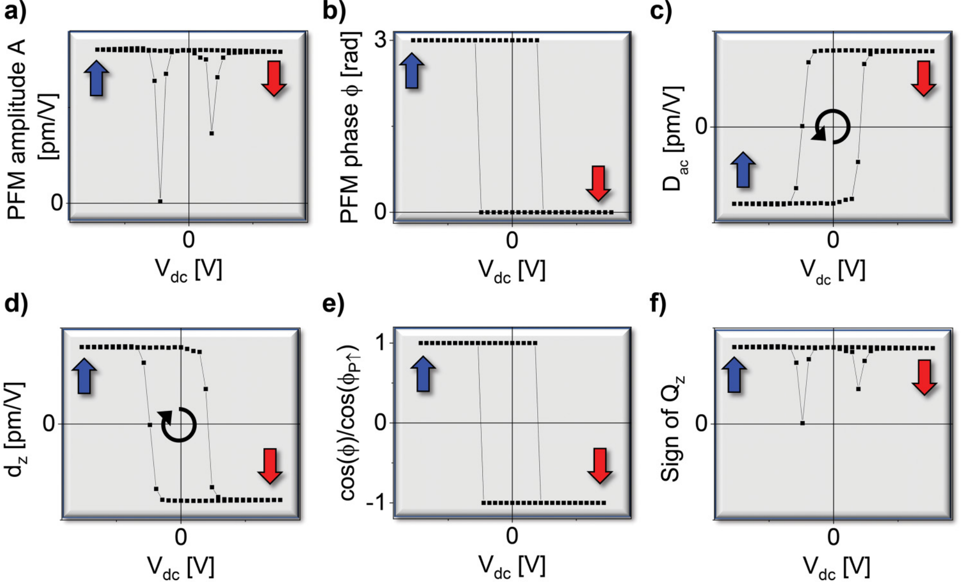


**FIG. 2.** Schematic outline of the correlation of the piezoelectric constant, PFM phase, and PFM amplitude hysteresis loop for a material with a positive electrostrictive coefficient. (a) PFM amplitude $A$, (b) phase $\phi$, (c) mixed PFM signal $D_{ac}$, (d) piezoelectric coefficient $d_z$, (e) cos(ϕ)/cos(ϕ$_{P\uparrow}$), and (f) sign of the electrostrictive coefficient $Q_z$ as a function of $V_{dc}$ voltage. The blue and red arrows indicate upward and downward polarization orientations, respectively.

If the PFM amplitude and phase are combined according to $D_{ac} = A{\cdot}\cos(\phi)$, then the corresponding PFM hysteresis loop is oriented counterclockwise as shown in Fig. 2(c). According to Eq. (1), the loop of the effective piezoelectric coefficient as a function of voltage is then oriented clockwise [Fig. 2(d)]. Here, domains switched upward show a positive $d_z$ and domains switched downward have a negative $d_z$.

From the piezoelectric response loop, one can determine the sign of the electrostrictive coefficient if the orientation of the polarization vector is known. For example, applying a negative voltage to the tip switches the polarization vector upward. Therefore, we can normalize cos($\phi$), which contains the directional information of the mixed PFM signal, with the cosine of the polarization direction representing an upward oriented polarization vector. Consequently, an upward oriented polarization vector is defined as +1 and a downward oriented polarization vector is −1 [Fig. 2(e)]. If the piezoelectric constant loop is then divided by the normalization result, one obtains a signal that has a value proportional to the effective electrostrictive coefficient reflecting its sign [Fig. 2(f)]. In order to obtain a value for $Q_z$, knowledge about permittivity and polarization is required, which cannot be obtained in a PFM experiment. However, it is important to point out that the sign of the effective $Q_z$ contributing to the measured PFM signal manifests itself in the orientation of the PFM hysteresis loop.

After establishing what PFM hysteresis loops are expected based on the sign of the electrostrictive coefficient, we investigate the extraction of PFM amplitude and PFM phase for the example of resonance-enhanced PFM, which is often used to enhance the PFM signal for samples with a weak electromechanical response. The quantification of PFM amplitude, i.e., the conversion of $D_{ac}$ from volts to pm, is commonly performed using the cantilever static deflection sensitivity $S_c$, which is extracted from static force-distance curves and allows conversion of the detector signal from volts into meters. The following example demonstrates that this approach is not suited for resonance-enhanced PFM if measurements with cantilevers of different stiffnesses are compared. This is important since it is getting more common to perform measurements with stiff probes to reduce contributions from electrostatic effects.[48] The measurement was performed on-resonance and the PFM amplitude was extracted after SHO-fitting of the contact resonance peak. Figure 3(a) shows a PFM amplitude image of a ferrielectric $CuInP_2S_6$[49,50] (CIPS) sample, which is interspersed with a non-ferroelectric $In_{4/3}P_2S_6$ (IPS) phase yielding a zero PFM amplitude. When the exact same area is measured with two different cantilevers with stiffnesses of 2.3 N/m and 35.8 N/m, the measured PFM amplitudes vary greatly even under comparable contact forces [Fig. 3(b)]. In this case, the PFM amplitude in Fig. 3(b) was extracted only for the CIPS domains and multiplied by the cantilever sensitivity $S_c$, which results in noticeably lower values for the stiffer cantilever. This means that measurements with different probes may not be directly compared. The root cause of this problem is that PFM is using an optical beam deflection to track the cantilever deflection change, which is sensitive to the local slope of the cantilever not to the $z$-shift of the probe tip. If PFM is performed on resonance, the shape of the cantilever beam during the vibrations at the first eigenmode frequency is greatly dependent on cantilever geometry and stiffness and probe-sample contact stiffness. Also, this shape is different from the shape acquired during calibration of the probe sensitivity with static force-distance curves, when $z$-shifts of the probe tip are much larger.[51,52] A softer cantilever will "buckle" more in PFM measurements than a stiff cantilever, which will directly influence the measured piezoelectric response. This effect can be removed by additional signal processing with the knowledge of cantilever geometry and stiffness, as well as resonance frequencies and quality factors of the cantilever flexural vibrations in contact and out of contact with the sample. These parameters can be used to calculate the cantilever beam shape and to convert the cantilever slope at the point where the laser spot is placed into


Published under license by AIP Publishing.

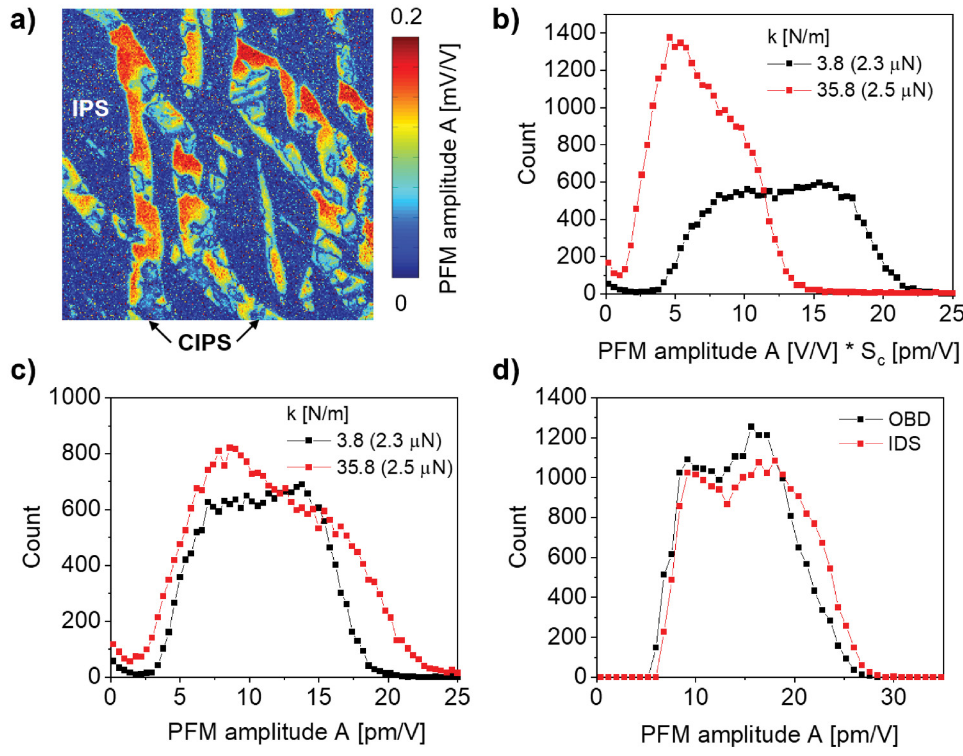


**FIG. 3.** (a) PFM amplitude map for a CIPS-IPS phase separated sample measured with a cantilever of 3.8 N/m stiffness. (b) PFM amplitude A measured in the same area with a soft and a stiff cantilever after quantification with cantilever sensitivity $S_c$. (c) PFM amplitude A measured in the same area with a soft and a stiff cantilever after correction based on cantilever dynamics.[41] (d) PFM amplitude A measured in the same area with IDS and OBD approaches including the correction procedure based on cantilever dynamics in the contact resonance.

sample surface displacements. The result is a shape correction factor that can be applied to the experimental data to remove the influence of the cantilever properties.[52,53] Alternatively, PFM techniques using laser Doppler vibrometers or interferometric displacement sensing[21,22] have been developed to gain fully quantitative information on the PFM amplitude but require additional hardware.

After application of a correction factor based on cantilever dynamics as demonstrated by Balke *et al.*,[52] the measured PFM amplitudes become comparable [Fig. 3(c)]. In a second example, interferometric displacement sensing (IDS) was used to measure the PFM amplitude and compared with a standard measurement using optical beam deflection (OBD) in the exact same area of a CIPS-IPS sample. After the cantilever dynamics calibration correction, both techniques show comparable values for the PFM amplitude, which demonstrate the importance of additional correction factors beyond cantilever sensitivity. Note that the shape correction method also applies to off-resonance techniques at low frequencies where the shape of the cantilever also depends on the properties of the cantilever and the tip-sample contact.

In the case of the PFM phase, the phase loop is sometimes shifted along the phase axis in the data processing to maximize the mixed response. The measured PFM phase of oppositely oriented polarization domains is rarely 0 and π rad, as schematically shown in Fig. 2, due to instrumental offsets including phase delays in cables, analog signal processing (e.g., by amplifiers and filters), cantilever dynamics, and experimental effects such as sample, tip-sample contact, and intrinsic material properties. The instrumental phase offsets can vary significantly and are investigated independent of ferroelectric signal contributions. Toward this goal, we measured the amplitude and phase using internal $V_{ac}$ sources, where a source output was used as a signal input on the same atomic force microscope (AFM) controller and discovered a strong dependency of the amplitude and phase on the ac frequency without the presence of a probe [Figs. 4(a) and 4(b), respectively]. While the amplitude is a non-linear function of frequency, the phase changes nearly linearly with frequency. This dependence is a common property for all commercial AFMs and affects all frequency-dependent measurements including non-contact and contact mode cantilever vibrations, as shown in Figs. 4(c) and 4(d). We studied the response for several different cantilevers of different stiffnesses by means of cantilever resonances (in non-contact and contact modes) to cover a large frequency range and analyzed the phase to the left of the resonance at the lower end of the 10 kHz-wide frequency window $f_{min}$ [Fig. 4(c)]. The result is plotted in Fig. 4(d) and demonstrates that the behavior of the frequency-dependent phase offset is similar for the electrostatically driven cantilever vibrations for $SiO_2$ or piezoelectrically driven cantilever vibrations for PZT. Strong linear dependency is observed in both the cases, and in the case of PZT, the two parallel lines are separated by π and correspond to upward and downward oriented domains on PZT.

The origin of the above discussed instrumental phase offset is believed to be instrument electronics, sampling delays, and even the cables. Additional phase offsets can be introduced when cantilever dynamics are involved. Therefore, the slope of the linear frequency–phase relationship can vary for different microscopes and


Published under license by AIP Publishing.

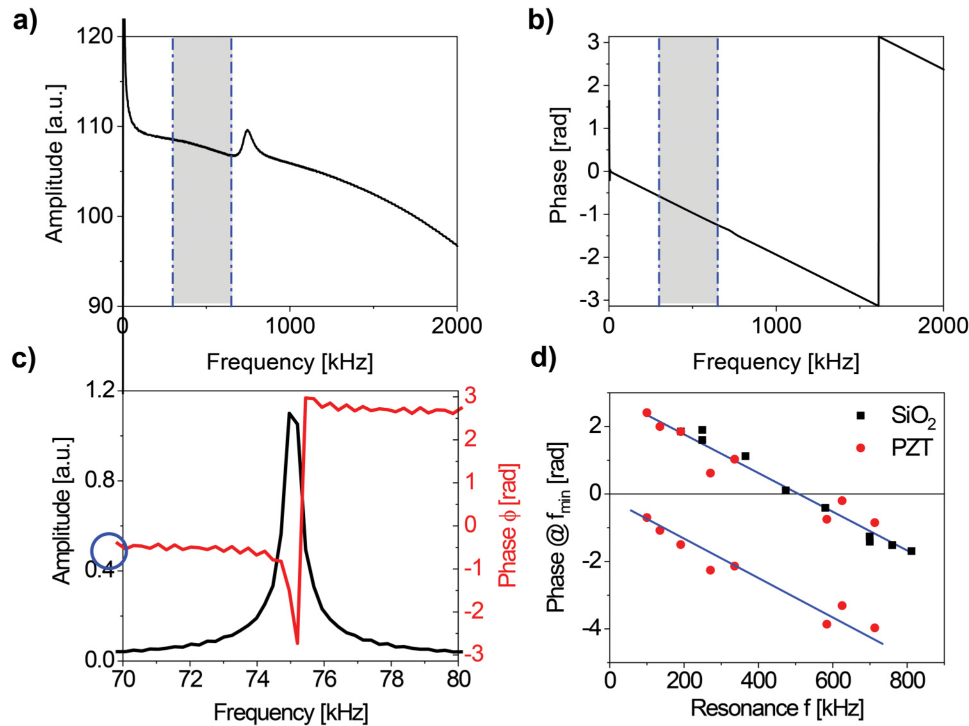


FIG. 4. Amplitude- and phase-frequency characteristics: (a) and (b) purely instrumental—in the absence of a cantilever and (c) and (d) measured in a PFM setup with the piezo-effect or electrostatic driving. (a) Amplitude and (b) phase as a function of frequency using output of an internal $V_{ac}$ source, which was routed back into the AFM controller as the input signal. (c) Cantilever amplitude and phase across the resonance frequency for an electrostatically driven cantilever above a $SiO_2$ sample (in the non-contact mode). (d) Phase at $f_{min}$ [as indicated by the blue circle in (c)] as a function of frequency for electrostatically driven cantilever vibrations for $SiO_2$ (non-contact and contact mode) and piezo-electrically driven vibrations for the PZT, collected with many cantilevers of different stiffnesses. The two bands for PZT, which are separated by $\pi$, are measured on upward and downward oriented domains.

experimental setups. This results in varying slopes in the phase as a function of frequency. The instrumental phase offsets can become so large that measurements with different cantilevers can change the PFM loop orientation. For example, in order to reduce electrostatic signal contributions, it has been suggested to use stiffer tips.[29] For the resonance-enhanced PFM, however, this increases the measurement frequency. Based on the cantilever properties, the higher operating frequency can lead to a complete flip of the PFM phase loop, which explains the opposite loop orientation as illustrated in Fig. 1(b).

We would like to emphasize that this frequency dependence of the phase has to be considered for both on- or off-resonance techniques. However, further considerations for the PFM phase need to be taken into account if measurements are performed at a contact resonance frequency to enhance the signal-to-noise ratio.[11,17] In resonance-enhanced techniques, the PFM amplitude and phase are captured across the contact resonance of the cantilever probe, which is determined by mechanical properties of the sample and cantilever as well as its geometry. Often, the contact resonance peak is fitted with a simple harmonic oscillator (SHO) equation from which the PFM amplitude $A$, quality factor $Q$, contact resonance frequency $f_c$, and PFM phase $\phi$ are extracted. The quality factor and resonance frequency provide further information on energy dissipation[17] and changes in mechanical properties.[54] The SHO-based analysis of the phase data is centered around three questions: (i) How accurately were the fit performed and the phase extracted? (ii) Is the signal-to-noise (S/N) ratio high enough for a meaningful fitting? and (iii) Does the SHO model adequately describe the measured data?

There are two approaches that are most often used to extract the PFM phase from SHO fits, and we have applied them here for fitting a cantilever resonance peak to illustrate a difference in outcomes of the methods. First, only the amplitude peak is fitted using Eq. (3), and the phase is extracted at the contact resonance frequency [Fig. 5(a)], resulting in a PFM phase value of $\phi = 2.67$ rad for the used dataset,

$$A = A_0 \cdot \frac{f_c^2}{\sqrt{(f^2 - f_c^2)^2 + \left(\frac{f \cdot f_c}{Q}\right)^2}}, \tag{3}$$

$$D_{ac} = A_0 \cdot f_c^2 \cdot e^{i\phi} / (f^2 - (i\, f\, f_c/Q) - f_c^2). \tag{4}$$

Second, a 3D-SHO fit of the real and imaginary responses as a function of frequency can be performed, where the PFM phase $\phi$ is one of the fitting parameters [Fig. 5(b)] resulting in a PFM phase value of $\phi = 1.23$ rad using Eq. (4). In both equations, $f_c$ denotes the contact resonance frequency, $Q$ is the quality factor, and $A_0$ is the PFM amplitude. Therefore, different data analysis methods can result in different PFM phase values. This is simply based on the fact that in the 2D plot, the PFM phase is defined as the phase at the contact resonance frequency, whereas the 3D model shown here extracts the phase on the low-frequency side of the contact resonance peak. It is important to realize that different methods of SHO fit result in a different PFM phase, which is important when different measurements are compared. Another factor that can


Published under license by AIP Publishing.

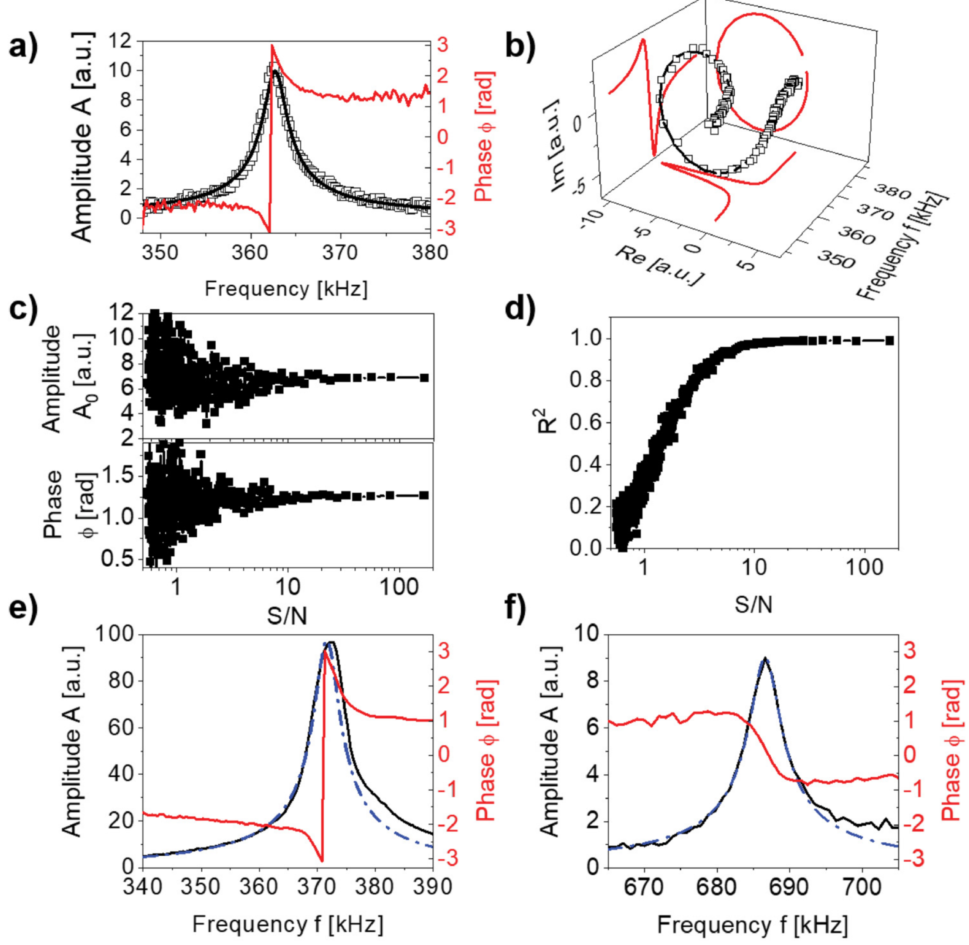


**FIG. 5.** Phase and amplitude across the contact resonance in (a) 2D and (b) 3D parameter space. (c) PFM amplitude and phase extracted from a 3D SHO fit with artificial noise. (d) $R^2$ value for the SHO fits as a function of the signal to noise ratio. Deviation from the standard SHO in the form of (e) an asymmetric amplitude peak and (f) non-π phase shift across the resonance.

influence the SHO fitting parameters is the S/N ratio. We demonstrate the importance of the S/N ratio for the PFM amplitude and phase [Fig. 5(c)] by overlaying the data shown in Fig. 5(b) with artificial noise of varying magnitude and subsequent SHO fitting. Both fitted amplitude and phase clearly become unreliable if the S/N ratio is too small. In addition, the coefficient of determination, $R^2$, provides a measure for the fitting quality and is shown in Fig. 5(d) for the same S/N ratios. The $R^2$ coefficient increases with increasing S/N ratios, and a value close to 1 is desirable. This value can be used to exclude unreliable data points. In particular, near coercive voltages, the S/N ratio can significantly decrease due to the low PFM response. Hence, care must be exercised when imposing physical interpretation on fitting parameters $A$, $\phi$, $f_c$, and $Q$ in the vicinity of switching events. The effects of lower S/N ratios can be mitigated by improving initial guesses in the fitting algorithm or using a deep neural network approach.[62] In addition to the consideration of signal strength and noise levels, it is equally important to understand how well the SHO equation describes the actual resonance. Asymmetric amplitude peak shapes can arise from mechanical non-linearity, electrical crosstalk between the drive and response, and non-piezoelectric signal contribution,[55] which are not captured by the SHO fit [Fig. 5(e)]. The same is true for the PFM phase change across the resonance, which can deviate from π [Fig. 5(f)]. This type of behavior can be observed when stiff probes are used to perform PFM experiments on non-ferroelectric samples where electrostatic forces alone drive the cantilever motion. Both deviations in amplitude and in phase from the SHO model lead to systematic errors in the determination of the PFM response.

If the instrumental phase offset and the phase extraction from the SHO fitting procedure are unknown, a sample with a known sign of electrostrictive coefficient, $Q$, can be used as a reference in combination with systematic rules for PFM phase correction. Once established, the same phase correction offset can be applied to materials with unknown sign of the electrostrictive constant if the measurement setup and cantilever are not changing. This also applies to off-resonance PFM methods. Since PFM contains information about the strength of the piezoelectric response and the direction of polarization, a material with a positive electrostrictive coefficient can show positive or negative values in PFM measurements [Eq. (2)]. The same is true for materials with a negative electrostrictive coefficient. Therefore, additional information is necessary to uncouple the sign of the electrostrictive coefficient from


Published under license by AIP Publishing.

the polarization direction since the measured sign of the piezoelectric material response is a convolution of both. If the polarization orientation is unknown or varies locally, poling experiments can help to obtain a reference domain. In the following discussion, all measurements were obtained with cantilevers that have a stiffness of 3–4 N/m and a contact resonance frequency of 330–360 kHz. Here, we performed the resonance-enhanced PFM imaging after local areas of a 60 nm $PbZr_{0.2}Ti_{0.8}O_3$/20 nm $SrRuO_3$/$TbScO_3$ (110) thin film heterostructure had been poled with ±3 V, as indicated in Fig. 5(a). Here, "positive" or "up" refers to the positive *z*-direction (pointing away from the substrate), whereas "negative" or "down" refers to the negative *z*-direction (pointing toward the substrate). A negative voltage applied to the tip in respect to the bottom electrode results in an electric field pointing up, which switches the polarization direction upwards, while a positive voltage switches it downward. Based on this principle, we expect the PFM phase in the area poled by applying a negative voltage to have an out-of-phase response with $\phi = \pi$ as discussed in Fig. 2. Conversely, in the positively poled area (polarization orientation down), an in-phase response with $\phi = 0$ [Fig. 6(b)] should be detected. The extracted PFM amplitude and phase plotted as a 2D histogram [Fig. 6(c)] shows PFM phase values of approximately −2.4 rad for the positively poled area and ∼0.7 rad for the negatively poled one after using a 3D fit model to extract the PFM phase from the SHO fit; neither provides the expected values of 0 and 3.14, respectively. Therefore, the phase has to be offset by $\phi_{\mathrm{offset}} = -2.4$ rad, and $A{\cdot}\cos(\phi\text{-}\phi_{\mathrm{offset}})$ should be used to calculate the mixed-PFM response. The impact of the result without and with the PFM phase correction is shown in Figs. 6(d) and 6(e), respectively. Besides the lower $D_{ac}$ values for the case without phase correction, most notable is the contrast inversion. For example, the central domain is oriented downward based on the applied poling voltage of 3 V. However, $D_{ac}$ is negative when no phase offset is applied, which would indicate a domain with an upward polarization according to the working principle of PFM [Fig. 2(c)]. Once the correct phase offset is applied, the PFM contrast is aligned with the expected polarization orientation after poling. Using this poling procedure as a means to determine the phase offset does require a ferroelectric sample with stable domains of polarization which orients according to the applied electric field.

The summary of the proposed steps toward more reliable and quantified PFM measurements is shown in Fig. 7. The technique is based on using a reference sample as the calibration method,

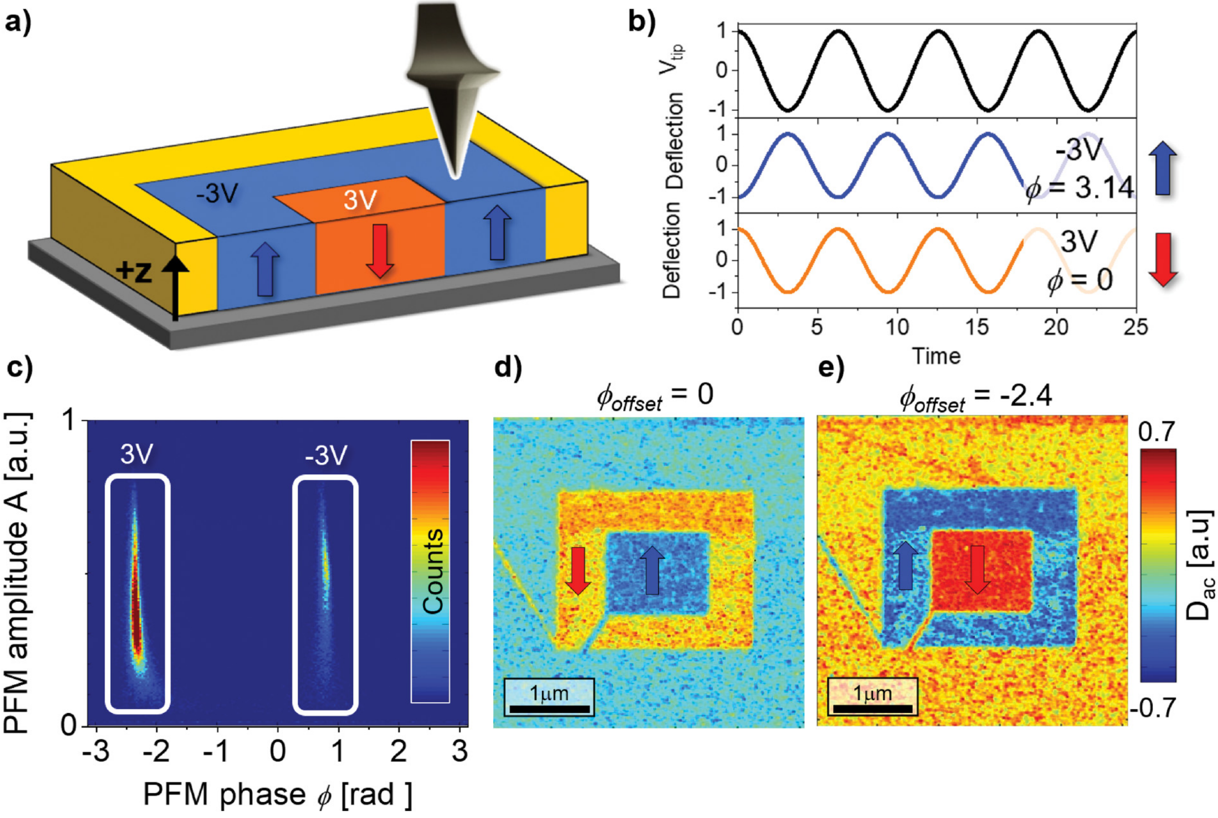


**FIG. 6.** (a) Schematic image of the PFM poling experiment (the bias voltage is applied to the probe) and (b) the expected in- or out-of-phase responses based on the polarization orientation. (c) Measured PFM amplitude and phase plotted as a 2D histogram. Map of the mixed PFM response in a 5 × 5 $\mu m^2$ area without (d) and with (e) phase offset.


Published under license by AIP Publishing.

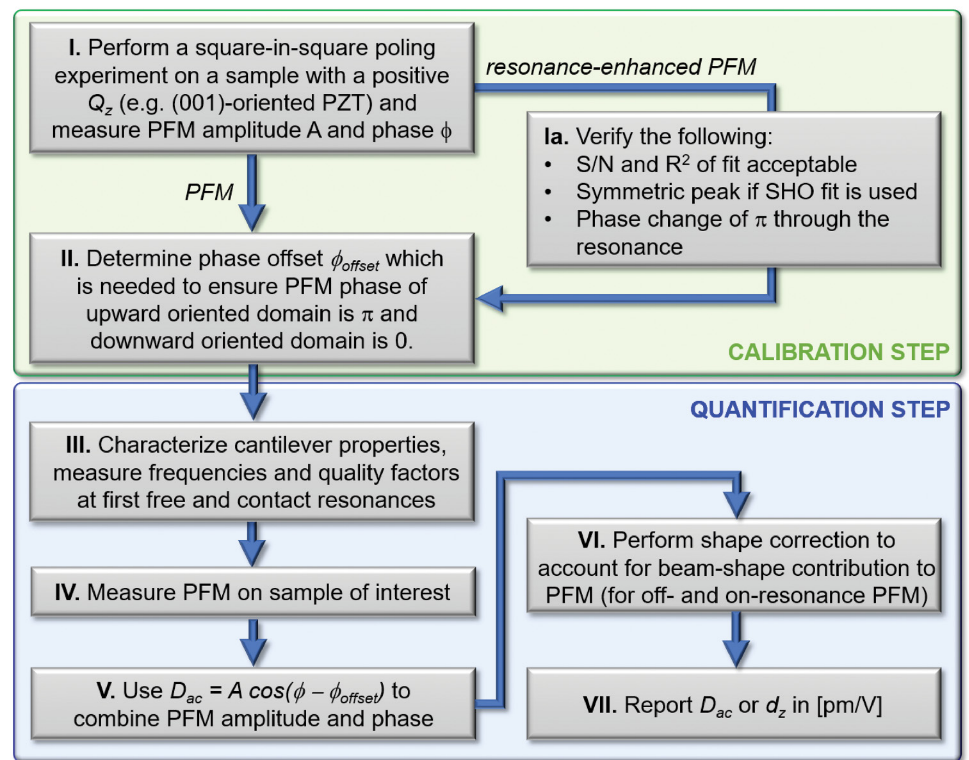


FIG. 7. Summary of recommended PFM calibration and quantification steps for off- and on-resonance PFM.

instead of measuring instrumental phase offsets, and highlights additional steps needed for the resonance-enhanced PFM methods. It is possible to determine the PFM phase offset also from PFM hysteresis loop measurements if it is warranted that complete ferroelectric switching occurs and that the signal of the piezoelectric origin is the main contributor to the measured PFM signal. The suggested procedure has been tested on two samples. A 50 nm thick ferroelectric (001) $Pb(Zr_{0.2}Ti_{0.8})O_3$ (PZT)/(La,Sr)$MnO_3$ film grown epitaxially with pulsed laser deposition on an $SrTiO_3$ (001) substrate with a positive effective electrostrictive coefficient along the $z$ axis was used as a reference sample. The second sample was an oriented $CuInP_2S_6$ (CIPS) crystal that was aligned so that the crystallographic $c$ axis is normal to the sample surface, and hence, the effective electrostrictive coefficient along the $z$ axis is determined by the $Q_{3333}$ component of the electrostrictive tensor and negative.[43,44] Resonance-enhanced PFM hysteresis loops were measured off-field, that is, after the application of dc voltage pulses to the probe to initiate domain switching. The resulting $d_z$ loops after the application of the phase calibration show the expected loop orientations for the respective sign of the electrostrictive coefficient, i.e., clockwise for positive [Fig. 8(a)] and counterclockwise for negative $Q_z$ [Fig. 8(b)]. It should be emphasized that the outlined

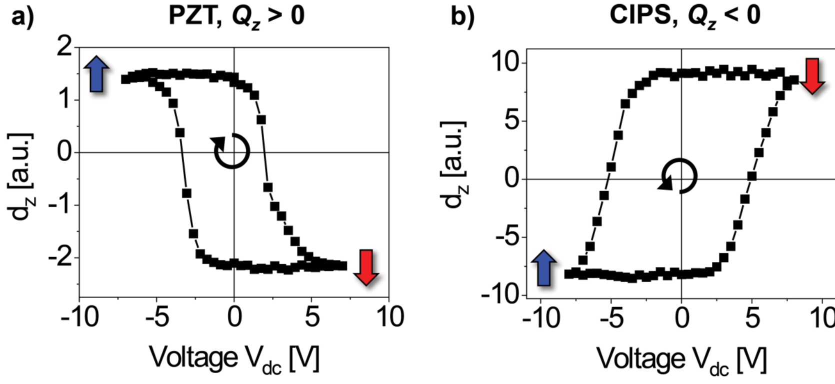


FIG. 8. Piezoelectric constant loops extracted from PFM response as a function of applied $V_{dc}$ as outlined in this work for a material with a (a) positive and (b) negative electrostrictive constant.


Published under license by AIP Publishing.

considerations about the PFM phase are only valid for the specified frequency at which PFM is measured (330–360 kHz). As previously discussed, if measurements are performed with a stiffer tip at high enough frequencies to cause the phase to change sign, the outlined methodology will need to be adjusted to work in this new frequency range. The same is true if on-field PFM hysteresis loops are measured where additional signal generating mechanisms (such as electrostatic forces) can affect and even reverse the measured phase values. If poling experiments are not feasible, similar approaches can be applied for bias-dependent PFM hysteresis loops. Alternative strategies can include measuring internal phase offsets for mechanically driven cantilever, for example, through the use of BlueDrive[56] before performing PFM.

While the proposed methodology will apply to many PFM investigations of ferroelectric materials, there are situations where they do not apply. The existence of field components perpendicular to the surface normal and the inhomogeneous field distribution around the biased PFM tip result in multiple piezoelectric tensor components contributing to the measured $d_z$.[27] These in-plane contributions can be comparable with the out-of-plane contributions and can result in a negative effective piezoelectric constant even if the effective electrostrictive coefficient is positive as, for example, was shown for the case of $Bi_4Ti_3O_{12}$ nanorods.[57] Therefore, it is important to consider the crystallographic sample orientation and piezoelectric tensor components when evaluating the measured PFM signal. In addition, the proposed calibration method will not work for abnormal polarization switching[58,59] or in instances where mechanical poling plays a significant role.[60] Besides the sign of the effective electrostrictive coefficient, the laser spot of the optical beam on the cantilever can also determine the orientation of the PFM hysteresis loop.[61] This has to do with the fact, for example, that the beam shape for the first eigenmode has comparable slopes on the front and back halves of the cantilever but with opposite signs.

## III. SUMMARY

In summary, we highlighted the importance of correct processing of the PFM amplitude and phase signals to achieve a higher degree of quantification accuracy and reproducibility with respect to the local piezoelectric strength and polarization orientation. The quantification of the PFM amplitude based on cantilever sensitivity is not sufficient, especially for stiffer cantilevers that are often used to reduce electrostatic signal contribution. The PFM phase determines the orientation of the PFM loops from which information on the sign of the measured piezoelectric and, thus, electrostrictive coefficient can be gained. PFM phase values can appear deviating from ideal 0 and π, which can lead to wrongfully oriented piezoelectric hysteresis loops. Accurate processing of the phase signal requires taking into account instrumental phase offsets that occur in virtually all PFM measurements for data processing and interpretation. This instrumental phase offset is dependent on frequency and must be assessed for each experimental setup separately (since it varies with factors like cantilever stiffness, signal routing, cabling, etc.). In addition, for the contact resonance-enhanced techniques, it is important to take into account the quality of the SHO fit and how the phase data are extracted. Specifically, in the presence of non-piezoelectric signal contributions, the SHO model may not describe the measured data well enough, e.g., if the peak shape is asymmetric or the phase change across the contact resonance is ≠π. Moreover, it should be assessed whether the S/N ratio is high enough for a proper fit. SHO fitting can be performed in several ways, e.g., fitting only the amplitude peak and extracting the phase at resonance vs fitting 3D data in the imaginary-real-frequency parameter space where the phase value is a fitting parameter and extracted at frequencies higher than the resonance frequency. Since the phase varies strongly across a resonance, it is important to know how/where the phase is extracted and to keep that procedure consistent. In the case presented here, it was necessary to zero the PFM phase level measured on domains with downward oriented polarization vector, so that the phase values are between 0 rad and 3.14 rad dependent on downward or upward polarization orientation, respectively. This convention is in accordance with the working principle of PFM linking periodic in-phase and out-of-phase mechanical deformations in response to an AC electric field. The mixed response $D_{ac}$ should then be calculated as $D_{ac} = A\cos(\phi + \phi_{\text{offset}})$ and is coupled with the piezoelectric coefficient $d$ by a factor of $-1$. If these outlined steps are followed, material parameters such as the amplitude and the sign of the electrostrictive constant can be inferred from the $D_{ac}$ and $d$ images as well as the orientation of the measured hysteresis loops as a function of applied voltage.

## ACKNOWLEDGMENTS

The experiments in this work were performed and supported at the Center for Nanophase Materials Sciences in Oak Ridge National Lab, which is a DOE Office of Science user facility (L.C., S.J., S.V.K., and N.B.). The measurements on the PZT sample were supported by the Division of Materials Science and Engineering, Basic Energy Sciences, U.S. Department of Energy (S.M.N.). S.S. acknowledges support from the National Science Foundation (NSF) under Grant No. DMR-1708615 for PZT synthesis. L.W.M. acknowledges support from the Army Research Office under Grant No. W911NF-14-1-0104 for PZT synthesis. In part (A.T.), this work was developed within the scope of the project CICECO-Aveiro Institute of Materials, Nos. UIDB/50011/2020 and UIDP/50011/2020, financed by national funds through the Portuguese Foundation for Science and Technology/MCTES.

## DATA AVAILABILITY

The data shown in this tutorial are available from the corresponding author upon reasonable request.

## REFERENCES

[1] S. V. Kalinin, B. J. Rodriguez, S. Jesse, E. Karapetian, B. Mirman, E. A. Eliseev, and A. N. Morozovska, Ann. Rev. Mater. Res. **37**, 189 (2007).
[2] S. V. Kalinin, B. J. Rodriguez, S. Jesse, E. Karapetian, B. Mirman, E. A. Eliseev, and A. N. Morozovska, Ann. Rev. Mater. Res. **37**(1), 189–238 (2007).
[3] N. Balke, I. Bdikin, S. V. Kalinin, and A. L. Kholkin, J. Am. Ceram. Soc. **92**, 1629 (2009).
[4] M. Alexe, A. Gruverman, C. Harnagea, N. D. Zakharov, A. Pignolet, D. Hesse, and J. F. Scott, Appl. Phys. Lett. **75**, 1158 (1999).
[5] D. A. Bonnell, S. V. Kalinin, A. L. Kholkin, and A. Gruverman, MRS Bull. **34**, 648 (2009).


Published under license by AIP Publishing.

[6] J. M. Gregg, Phys. Status Solidi A **206**, 577 (2009).
[7] S. V. Kalinin and D. A. Bonnell, Phys. Rev. B **65**, 125408 (2002).
[8] P. Maksymovych, S. Jesse, P. Yu, R. Ramesh, A. P. Baddorf, and S. V. Kalinin, Science **324**, 1421 (2009).
[9] A. Roelofs, I. Schneller, K. Szot, and R. Waser, Appl. Phys. Lett. **81**, 5231 (2002).
[10] M. H. Zhao, Z. L. Wang, and S. X. Mao, Nano Lett. **4**, 587 (2004).
[11] B. J. Rodriguez, C. Callahan, S. V. Kalinin, and R. Proksch, Nanotechnology **18**, 475504 (2007).
[12] M. Alexe, C. Harnagea, D. Hesse, and U. Gosele, Appl. Phys. Lett. **79**, 242 (2001).
[13] A. Gruverman and S. V. Kalinin, J. Mater. Sci. **41**, 107 (2006).
[14] A. Gruverman, B. J. Rodriguez, C. Dehoff, J. D. Waldrep, A. I. Kingon, R. J. Nemanich, and J. S. Cross, Appl. Phys. Lett. **87**, 082902 (2005).
[15] S. Jesse, A. P. Baddorf, and S. V. Kalinin, Appl. Phys. Lett. **88**, 062908 (2006).
[16] N. Setter, D. Damjanovic, L. Eng, G. Fox, S. Gevorgian, S. Hong, A. Kingon, H. Kohlstedt, N. Y. Park, G. B. Stephenson, I. Stolitchnov, A. K. Taganstev, D. V. Taylor, T. Yamada, and S. Streiffer, J. Appl. Phys. **100**, 051606 (2006).
[17] E. A. Eliseev, S. V. Kalinin, S. Jesse, S. L. Bravina, and A. N. Morozovska, J. Appl. Phys. **102**, 014109 (2007).
[18] S. Jesse, S. V. Kalinin, R. Proksch, A. P. Baddorf, and B. J. Rodriguez, Nanotechnology **18**, 435503 (2007).
[19] N. Balke, P. Maksymovych, S. Jesse, A. Herklotz, A. Tselev, C.-B. Eom, I. I. Kravchenko, P. Yu, and S. V. Kalinin, ACS Nano **9**, 6484 (2015).
[20] R. K. Vasudevan, N. Balke, P. Maksymovych, S. Jesse, and S. V. Kalinin, Appl. Phys. Rev. **4**, 021302 (2017).
[21] A. Labuda and R. Proksch, Appl. Phys. Lett. **106**, 253103 (2015).
[22] L. Collins, Y. Liu, O. S. Ovchinnikova, and R. Proksch, ACS Nano **13**, 8055 (2019).
[23] S. Alexander, L. Hellemans, O. Marti, J. Schneir, V. Elings, P. K. Hansma, M. Longmire, and J. Gurley, J. Appl. Phys. **65**, 164 (1989).
[24] G. Meyer and N. M. Amer, Appl. Phys. Lett. **53**, 1045 (1988).
[25] S. Lei, E. A. Eliseev, A. N. Morozovska, R. C. Haislmaier, T. T. A. Lummen, W. Cao, S. V. Kalinin, and V. Gopalan, Phys. Rev. B **86**, 134115 (2012).
[26] S. V. Kalinin, B. J. Rodriguez, S. Jesse, J. Shin, A. P. Baddorf, P. Gupta, H. Jain, D. B. Williams, and A. Gruverman, Microsc. Microanal. **12**, 206 (2006).
[27] S. V. Kalinin, E. A. Eliseev, and A. N. Morozovska, Appl. Phys. Lett. **88**, 232904 (2006).
[28] H. Han, Y. J. Park, S. Baik, W. Lee, M. Alexe, D. Hesse, and U. Gosele, J. Appl. Phys. **108**, 044102 (2010).
[29] S. Kim, D. Seol, X. L. Lu, M. Alexe, and Y. Kim, Sci. Rep. **7**, 41657 (2017).
[30] M. C. Rodriguez-Aranda, F. Calderon-Pinar, F. J. Espinoza-Beltran, F. J. Flores-Ruiz, E. Leon-Sarabia, R. Mayen-Mondragon, and J. M. Yanez-Limon, J. Mater. Sci. Mater. Electron. **25**, 4806 (2014).
[31] J. S. Yang, S. H. Kim, J. H. Yeom, C. Y. Koo, C. S. Hwang, E. Yoon, D. J. Kim, and J. Ha, Integr. Ferroelectr. **54**, 515 (2003).
[32] T. Jungk, A. Hoffmann, and E. Soergel, Appl. Phys. Lett. **91**, 253511 (2007).
[33] T. Jungk, A. Hoffmann, and E. Soergel, Appl. Phys. A Mater. Sci. Process. **86**, 353 (2007).
[34] Q. N. Chen, S. B. Adler, and J. Li, Appl. Phys. Lett. **105**, 201602 (2014).
[35] S. Bradler, S. R. Kachel, A. Schirmeisen, and B. Roling, J. Appl. Phys. **120**, 165107 (2016).
[36] B. Bhatia, J. Karthik, D. G. Cahill, L. W. Martin, and W. P. King, Appl. Phys. Lett. **99**, 173103 (2011).
[37] J. Jiang, Y. Bitla, C. W. Huang, T. H. Do, H. J. Liu, Y. H. Hsieh, C. H. Ma, C. Y. Jang, Y. H. Lai, P. W. Chiu, W. W. Wu, Y. C. Chen, Y. C. Zhou, and Y. H. Chu, Sci. Adv. **3**, e1700121 (2017).
[38] Y. Luo, X. Y. Li, L. Chang, W. X. Gao, G. L. Yuan, J. Yin, and Z. G. Liu, AIP Adv. **3**, 122101 (2013).
[39] Q. Yu, J. F. Li, F. Y. Zhu, and J. Y. Li, J. Mater. Chem. C **2**, 5836 (2014).
[40] X. Y. Zhang, M. Y. Kang, K. R. Huang, F. Y. Zhang, S. X. Lin, X. S. Gao, X. B. Lu, Z. Zhang, and J. M. Liu, Nanoscale Res. Lett. **10**, 1028 (2015).
[41] N. Balke, S. Jesse, B. Carmichael, M. B. Okatan, I. I. Kravchenko, S. V. Kalinin, and A. Tselev, Nanotechnology **28**, 065704 (2017).
[42] I. Katsouras, K. Asadi, M. Y. Li, T. B. van Driel, K. S. Kjaer, D. Zhao, T. Lenz, Y. Gu, P. M. Blom, D. Damjanovic, M. M. Nielsen, and D. M. de Leeuw, Nat. Mater. **15**, 78 (2016).
[43] S. M. E. Neumayer, A. Eugene, M. A. Susner, A. Tselev, B. J. Rodriguez, S. Jesse, S. V. Kalinin, M. A. McGuire, A. N. Morozovska, P. M. Maksymovych, and N. Balke, Phys. Rev. Mater. **3**, 024401 (2019).
[44] L. You, Y. Zhang, S. Zhou, A. Chaturvedi, S. A. Morris, F. Liu, L. Chang, D. Ichinose, H. Funakubo, W. Hu, T. Wu, Z. Liu, S. Dong, and J. Wang, Sci. Adv. **5**, eaav3780 (2019).
[45] F. Liu, L. You, K. L. Seyler, X. Li, P. Yu, J. Lin, X. Wang, J. Zhou, H. Wang, and H. He, Nat. Commun. **7**, 12357 (2016).
[46] A. F. Devonshire, Philos. Mag. **40**, 1040 (1949).
[47] A. F. Devonshire, Philos. Mag. **42**, 1065 (1951).
[48] A. Gomez, T. Puig, and X. Obradors, Appl. Surf. Sci. **439**, 577 (2018).
[49] M. A. Susner, M. Chyasnavichyus, A. A. Puretzky, Q. He, B. S. Conner, Y. Ren, D. A. Cullen, P. Ganesh, D. Shin, H. Demir, J. W. McMurray, A. Y. Borisevich, P. Maksymovych, and M. A. McGuire, ACS Nano **11**, 7060 (2017).
[50] M. A. Susner, A. Belianinov, A. Borisevich, Q. He, M. Chyasnavichyus, H. Demir, D. S. Sholl, P. Ganesh, D. L. Abernathy, and M. A. McGuire, ACS Nano **9**, 12365 (2015).
[51] A. Raman, J. Melcher, and R. Tung, Nano Today **3**, 20 (2008).
[52] N. Balke, S. Jesse, P. Yu, B. Carmichael, S. V. Kalinin, and A. Tselev, Nanotechnology **27**, 425707 (2016).
[53] J. P. Killgore, A. Deolia, L. Robins, and T. W. Murray, Appl. Phys. Lett. **114**, 133108 (2019).
[54] Q. Li, Y. Cao, P. Yu, R. K. Vasudevan, N. Laanait, A. Tselev, F. Xue, L. Q. Chen, P. Maksymovych, S. V. Kalinin, and N. Balke, Nat. Commun. **6**, 8985 (2015).
[55] N. Balke, S. Jesse, Q. Li, P. Maksymovych, M. B. Okatan, E. Strelcov, A. Tselev, and S. V. Kalinin, J. Appl. Phys. **118**, 072013 (2015).
[56] M. Kocun, A. Labuda, A. Gannepalli, and R. Proksch, Rev. Sci. Instrum. **86**, 083706 (2015).
[57] M. Azodi, C. Harnagea, V. Buscaglia, M. T. Buscaglia, P. Nanni, F. Rosei, and A. Pignolet, IEEE Trans. Ultrason. Ferroelectr. Freq. Control **59**, 1903 (2012).
[58] M. Abplanalp, J. Fousek, and P. Gunter, Phys. Rev. Lett. **86**, 5799 (2001).
[59] A. Y. Wu, P. M. Vilarinho, D. Wu, and A. Gruverman, Appl. Phys. Lett. **93**, 262906 (2008).
[60] H. Lu, C. W. Bark, D. E. de los Ojos, J. Alcala, C. B. Eom, G. Catalan, and A. Gruverman, Science **336**, 59 (2012).
[61] A. V. Ievlev, E. V. Nikolaeva, E. I. Shishkin, and V. Y. Shur, Ferroelectrics **398**, 26 (2010).
[62] N. Borodinov, S. Neumayer, S. V. Kalinin, O. S. Ovchinnikova, R. K. Vasudevan, and S. Jesse, NPJ Comput. Mater. **5**, 25 (2019).



Published under license by AIP Publishing.